Probing the evolution of antiferromagnetism in multiferroics

M. B. Holcomb,[1,2] L. W. Martin,[3,4] A. Scholl,[5] Q. He,[1] P. Yu,[1] C.-H. Yang,[1] S. Y. Yang,[1] P.-A. Glans,[5] M. Valvidares,[3] M. Huijben,[6] J. B. Kortright,[5] J. Guo,[5] Y.-H. Chu,[1,7] and R. Ramesh[1,3,8,*]

[1]*Department of Physics, University of California–Berkeley, Berkeley, California 94720, USA*

[2]*Department of Physics, West Virginia University, Morgantown, West Virginia 26506, USA*

[3]*Materials Science Division, Lawrence Berkeley National Laboratory, Berkeley, California 94720, USA*

[4]*Department of Materials Science and Engineering, Frederick Seitz Materials Research Laboratory, University of Illinois at Urbana–Champaign, Urbana, Illinois 61801, USA*

[5]*Advanced Light Source, Lawrence Berkeley National Laboratory, Berkeley, California 94720, USA*

[6]*Faculty of Science and Technology, MESA+ Institute for Nanotechnology, University of Twente, Enschede 7500 AE, The Netherlands*

[7]*Department of Materials Science and Engineering, National Chiao Tung University, HsinChu, Taiwan 30010, Republic of China*

[8]*Department of Materials Science and Engineering, University of California–Berkeley, Berkeley, California 94720, USA*

(Received 29 June 2009; revised manuscript received 4 March 2010; published 6 April 2010)

This study delineates the evolution of magnetic order in epitaxial films of the room-temperature multiferroic $BiFeO_3$ system. Using angle- and temperature-dependent dichroic measurements and spectromicroscopy, we have observed that the antiferromagnetic order in the model multiferroic $BiFeO_3$ evolves systematically as a function of thickness and strain. Lattice-mismatch-induced strain is found to break the easy-plane magnetic symmetry of the bulk and leads to an easy axis of magnetization which can be controlled through strain. Understanding the evolution of magnetic structure and how to manipulate the magnetism in this model multiferroic has significant implications for utilization of such magnetoelectric materials in future applications.

DOI: 10.1103/PhysRevB.81.134406 PACS number(s): 75.70.Ak, 75.50.Ee, 78.70.Dm, 77.80.Dj

Magnetoelectric multiferroics are the focus of much experimental and theoretical research[1–5] due to their potential to greatly impact emerging fields of study such as spin-based electronics (spintronics) and new forms of magnetic storage, logic, and memory devices.[5,6] An ideal multiferroic would be a ferroelectric, ferromagnet that exhibits strong coupling between these order parameters at room temperature. To date, such a material system has not emerged; instead, there is a strong focus on antiferromagnetic, ferroelectrics such as $BiFeO_3$ (BFO) that can be coupled to ferromagnetic materials to achieve the desired coupling between electric fields and ferromagnetism at room temperature.[6–10]

To enable the design of such devices based on multiferroics, it is essential to understand the nature of the various order parameters especially in thin-film samples. While conventional measurements, such as scanning probe microscopy and quantitative polarization-electric field measurements can probe the evolution of the ferroelectric order parameter, probing the corresponding antiferromagnetic component in a multiferroic material is only achievable through optical probes or neutron scattering.[1,11,12] Additionally, when a multiferroic is grown as an epitaxial thin film for potential device applications, the antiferromagnetic state can evolve as a function of the constraints imposed by reduced dimensionality as well as from the strain imposed by the substrate.[13] In this paper, we explore the evolution of antiferromagnetism, specifically the development of a preferred magnetic axis in thin films of the model multiferroic BFO using state-of-the-art photoemission based spectromicroscopy at the Advanced Light Source, Lawrence Berkeley National Laboratory.

BFO is one of the most widely studied multiferroic materials over the last decade largely because it is the only single-phase multiferroic material that is simultaneously both antiferromagnetic and ferroelectric at room temperature [Néel temperature $(T_N) \sim 643$ K and ferroelectric Curie temperature $(T_C) \sim 1103$ K].[14,15] This makes BFO an ideal candidate for use in room-temperature applications. BFO is a rhombohedrally distorted perovskite ferroelectric with large intrinsic polarization[16] and eight possible polarization directions occurring along the pseudocubic ⟨111⟩ body diagonals, one of which is shown in Fig. 1(a). It is also known to be a G-type, canted antiferromagnet,[16] which means that the individual

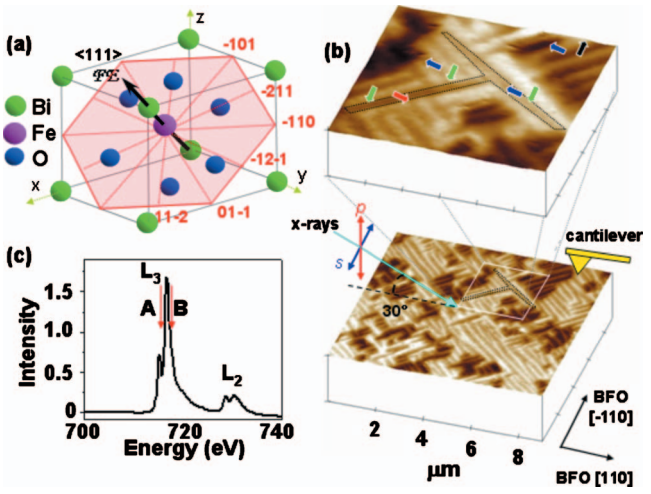

FIG. 1. (Color) Understanding order parameters in multiferroic BFO. (a) Schematic of (001)-oriented BFO crystal structure with polarization along ⟨111⟩ and predicted perpendicular easy magnetic plane for the bulk (shown as red hexagon). (b) PFM image of in-plane polarization projections with PFM and PEEM geometries (taken separately), showing incident x rays 30° from sample surface. (c) Absorption spectra of iron edge showing selected imaging energies.

moments on each Fe ion are aligned parallel within a given pseudocubic plane and antiparallel between adjacent planes. This plane is the perpendicular plane to the axis of rotation of the octahedra tilt,[17] which is also the polarization direction in most observed symmetries of both thin film and bulk BFO. Additionally, a Dzyaloshinskii-Moriya-type spin-orbital interaction gives rise to a canting of these moments and the observation of a weak ferromagnetic response.[18,19] Recent density-functional theory calculations for bulk BFO have predicted that the individual moments for each Fe ion should lie along any one of six possible energetically degenerate magnetic axes of the $\langle 1\bar{1}0\rangle$ or $\langle 112\rangle$ type in an easy 111-type plane, which is perpendicular to a given $\langle 111\rangle$-type polarization direction,[20] shown as the transparent red plane in Fig. 1(a). Thus, one critical question concerning magnetism in multiferroics such as BFO that is of both fundamental and technological importance is how this order parameter develops with strain and size effects? In this paper, we report that a systematic evolution of the state of magnetism is indeed accomplished through the imposition of a compressive (or tensile) strain on the bulk material. Our particular pathway is through an epitaxial constraint imposed by the substrate. We use angle-resolved, temperature-dependent photoemission electron microscopy (PEEM) to establish the fundamental nature of the magnetic state in BFO.

Single phase, epitaxial thin films of BFO were grown on a 50-nm-thick bottom electrode of $SrRuO_3$ (SRO) on $SrTiO_3$ (STO) (001) single-crystal substrates via laser-molecular-beam epitaxy and metalorganic chemical-vapor deposition. Detailed x-ray diffraction studies coupled with transmission electron microscopy were used to establish the crystalline quality of the heterostructures; these films were found to be single phase and fully epitaxial. This paper explores the evolution of magnetism that occurs in these BFO films. Throughout this paper we refer to two classes of films—thin films that have thickness (t) between 20 and 200 nm and thick films that have $t \sim 1$ μm.

A combination of in-plane and out-of-plane piezoresponse force microscopy (PFM) allows two-dimensional mapping of the ferroelectric polarization directions in a material.[21] Details of the measurements are reported by Zavaliche, *et al.*[21] The in-plane ferroelectric domain structure of a typical BFO thin film is shown in Fig. 1(b); the long axis of the ferroelectric domains (or direction of the domain walls) lies along the $\langle 100\rangle$ of the underlying STO (001) substrate or the pseudocubic $\langle 100\rangle$ of BFO. The polarization direction of the various stripelike domains lies along the $\langle 111\rangle$ and the in-plane projection of those polarization directions lie along the $\langle 110\rangle$. The arrows in Fig. 1(b) refer to the in-plane projection of the ferroelectric polarization directions (four variants) present in this model system. Such a model ferroelectric domain structure forms the reference frame for our photoemission measurements.

Synchrotron-based x-ray absorption and PEEM have emerged as powerful tools that provide chemically specific insight into the nature of magnetic order in materials.[22–24] Soft x-ray absorption experiments were performed at the elliptically polarizing undulator beamline 11.0.1 at the Advanced Light Source of Lawrence Berkeley National Laboratory. Samples were measured in total electron yield (TEY), which primarily collects inelastically scattered secondary electrons. The TEY sampling depth is $\sim 5-10$ nm. The photoemitted electrons were extracted into an electron-optical imaging system by an electric field that is applied between the sample and the first electrode of the electron-optical system. Several electron-optical lenses are used to form a full field image of the emitted electrons onto a phosphor screen, which is imaged by a charge-coupled-device camera. Magnetic domains can be observed by dividing intensity maps where the absorption is different among different domains or incident light polarizations. For this study, linear dichroic images were obtained at ± 0.5 eV from the Fe $L_{3,B}$ edge. The d-shell properties largely responsible for the magnetism of transition metals and oxides are probed through $2p$ to $3d$ dipole transitions, i.e., $L_{3,2}$ absorption spectra [Fig. 1(c)]. The L-edge spectra depend on anisotropies in the charge or the spin in the material, and thus are sensitive to the relative orientation of the x-ray polarization and antiferromagnetic axes which are then imaged by PEEM. Recognizing that x-ray linear dichroism (XLD) can arise from any anisotropic distribution of charge in a material (as would be the case for both ferroelectric and antiferromagnetic order), we have decoupled the contributions from these sources unambiguously through temperature- and angle-dependent measurements.

Figure 2(a) illustrates the x-ray polarization geometry in which the XLD-PEEM images in Figs. 2(b)–2(e) were taken. The images in Figs. 2(b)–2(e) are from the corresponding area shown in Fig. 1(b); for example, the "T" shaped domain in Figs. 1(b) and 2(b) is outlined as an aid to the reader. Images result from dividing intensity maps taken at the A and B multiplet peaks of the Fe L_3 absorption edge using linearly polarized light as the angle of the plane of linear incident polarization (α) varies from 0° (p polarization) to 90° (s polarization). The outlined arrows in Fig. 2 show the in-plane projection of the four ferroelectric directions. When the x rays are s polarized ($\alpha=90°$), only two contrast scales [labeled as light (1 and 3) and dark (2 and 4) in Fig. 2(b)] are observed. We have chosen a geometry such that the x-ray polarization vector for an s-polarized incident beam is along $[\bar{1}10]$, which maximizes the difference in intensity between the domains. In this geometry, the propagation vector of the incident x rays is nearly parallel to $[11\bar{1}]$ due to the $\theta=30°$ grazing angle from the sample surface [as shown in Fig. 2(a)]. Figures 2(b)–2(e) were obtained by changing the x-ray polarization angle α and keeping the grazing incidence angle θ fixed, which allowed us to gain insight into the magnetic structure by plotting the α-angle dependence of the x-ray dichroic signal. Individual ferroelectric polarization directions can be preferentially identified by rotating the x-ray polarization relative to the crystal as demonstrated in Fig. 2(c). For example, in Fig. 2(c), the technique highlights all $[\bar{1}1\bar{1}]$-type ferroelectric domains (black arrow). The angle dependence reveals that at $\alpha=70°$, three of the four $\langle 1\ 1\ 1\rangle$-type domains have similar contrast while the intensity from $[\bar{1}1\bar{1}]$ domains is much higher. Further rotation of the polarization to $\alpha=40°$ [Fig. 2(d)] results in an image where all four ferroelectric variants can be distinguished due to their differences in contrast. Contrast between certain do-

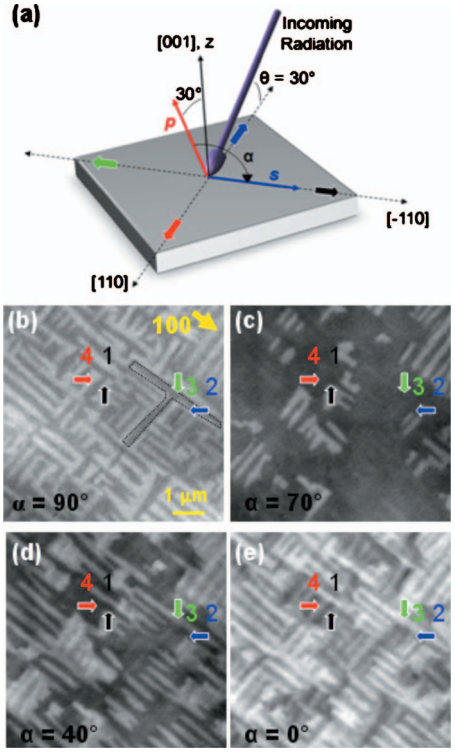

FIG. 2. (Color) PEEM images of BFO at several angles of the electric vector of incident linear polarization α. (a) Schematic illustrating the experimental geometries used to probe the angle-dependent linear dichroism in BFO. The outlined arrows show the in-plane projection of the four ferroelectric directions. Images of domain structures taken at (b) α=90°, (c) α=70°, (d) α=40°, and (e) α=0°.

main types can also vanish at other x-ray polarization angles—such as the $[1\bar{1}\bar{1}]$ and $[\bar{1}1\bar{1}]$-type domains in Fig. 2(e) for α=0.

Focusing on the image in Fig. 2(c), where we have controlled the relative orientation of the incidence x-ray polarization and the crystallographic orientation of BFO to preferentially observe one ferroelectric polarization direction (in this case all ferroelectric domains of the $[\bar{1}1\bar{1}]$ type), we gain insight into the nature of magnetism in BFO. We note again that all individual domains of a specific ferroelectric polarization direction exhibit identical contrast. This indicates that the antiferromagnetic order in a given set of identical ferroelectric domains is the same. This automatically rules out the possibility of a magnetic structure such as that in a bulk sample of BFO in which there is a 111-type easy plane of magnetization perpendicular to the polarization direction. PEEM imaging in this geometry would result in multiple contrast levels for a given set of identical ferroelectric domains if the antiferromagnetic domains were larger then the PEEM resolution (~30 nm). The formation of antiferromagnetic domains with sizes smaller than 30 nm is highly unlikely, purely due to energetic considerations, as is verified in the following measurements.[22] Therefore, the data in Fig. 2(c) is consistent with a magnetic structure in which an easy magnetic axis is formed in the {111}-magnetization plane of BFO similar to what is observed in strained NiO films.[25]

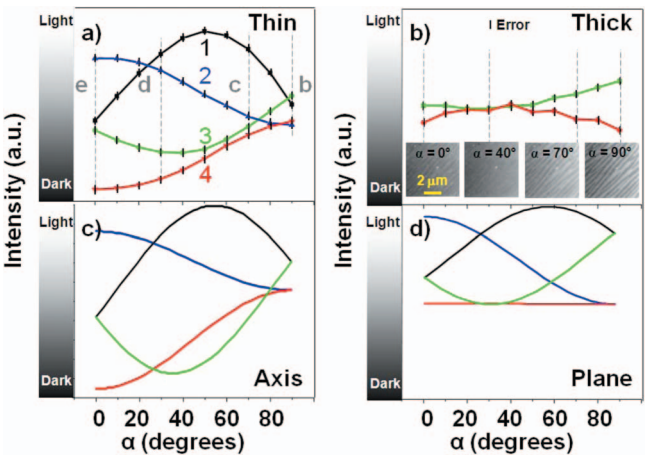

FIG. 3. (Color) Comparison between experimentally measured and modeled angle-dependent XLD contrast. Experimentally measured dichroic contrast as the x-ray polarization is rotated for both (a) thin and (b) thick BFO films. Error for all data points is less than 4% of the observed maximum contrast difference. The insets in (b) are the corresponding images for the data on the thick BFO films taken at the same experimental geometries as the thick films. Models of XLD contrast for two magnetic structures, (c) a unique magnetic axis and (d) an easy magnetic plane, are shown for the same sample orientation as in Fig. 2.

Simple models of the x-ray polarization angle (α) dependence of the dichroic domain contrast (Fig. 3) further support this conclusion. From a series of images [such as those in Figs. 2(b)–2(e)], we can extract the α dependence of dichroic contrast (from both ferroelectric and magnetic contributions) for thin [Fig. 3(a)] and thick [Fig. 3(b)] films and compare this data to model calculations as a function of the x-ray polarization angle α. The corresponding series of images for a prototypical thick BFO film have been included as an inset in Fig. 3(b) and illustrate similar stripelike images that correspond directly with PFM images. The PEEM images demonstrate no discernible magnetic variation within a given ferroelectric domain, illustrating the importance of the need to model different magnetic behaviors. The angle dependence of the magnetic contribution to linear dichroism of an antiferromagnet has been modeled[26] previously as

$$I = (3\cos^2\Theta_M - 1)\langle M^2\rangle_T, \quad (1)$$

where M is the magnetic moment at a temperature T and Θ_M is angle between the antiferromagnetic axis and the incident x-ray polarization vector axis. The ferroelectric contribution is also thought to exhibit a cosine-squared angular dependence[21,27] on the angle Θ_F between the ferroelectric polarization axis and the x-ray polarization axis. Therefore, we have modeled the dichroism from a multiferroic material with both magnetic and ferroelectric order when linearly polarized light is incident upon the sample at a given temperature as

$$I_{XLD} = P\cos^2\Theta_F + Q\cos^2\Theta_M, \quad (2)$$

where $|P|+|Q|=1$. Constants P and Q can be either positive or negative, where $|P|$ and $|Q|$ are, respectively, the percentage contribution of the polarization and magnetic components to the dichroism at the given temperature. We have considered both positive and negative values for the constants P and Q in the current study. The dashed lines in Fig. 3(a) correspond to the selected images in Fig. 2 and the colors of the curves match the in-plane projection of the ferroelectric directions and colored arrows displayed in Figs. 1(b) and 2. We have investigated a large number of possible magnetic structures encompassing many individual directions within the easy magnetization plane, combinations of these directions, and other possible directions not limited to that magnetization plane.

Models of the x-ray polarization angle dependence of the dichroic contrast for the two candidate magnetic structures previously discussed—a unique magnetic axis versus an easy magnetic plane—are shown in Figs. 3(c) and 3(d), respectively. By comparing the experimentally measured dichroic contrast [Figs. 3(a) and 3(b)] with that of the calculated angle dependencies, a clear correlation emerges. For thin films, the data clearly indicates an easy magnetic *axis* is present in the film while in contrast, for thick films, the data strongly suggests an easy magnetic *plane* is present. We note that data for only two variants are presented for the thick films due to experimental constraints in producing thick films with four variants. Regardless, clear differences in the magnetic structure between thin and thick BFO films are observed, presenting the first evidence for the formation of an easy or preferred magnetic axis in epitaxially strained thin films of BFO. It should be noted that small deviations between the experimentally observed data and these simple models could originate from the fact that only the dominating contributions to dichroism (in this case, magnetism and ferroelectricity) have been utilized in the study. Prior studies have suggested the importance of other factors, such as the orientation of the crystallographic axis.[28] These additional factors will not, however, change the major conclusions of this analysis.

The angle-dependent data and model for thin films of BFO [Figs. 3(a) and 3(c)] can only be achieved by two types of easy axes: $[1\bar{1}0]$ and [112] for a given $[11\bar{1}]$-polarization direction. The image contrast for these two scenarios can look the same due to the fact that P and Q in Eq. (2) are variables. However, previous temperature-dependent measurements have shown that the percentage of the dichroism at room temperature originating from the ferroelectric polarization (P) is approximately $60\pm10\%$.[29] Therefore, we present the results of our modeling from this range since it reasonably reflects the dependence of the observed data. In order to uniquely identify this axis, we have carried out temperature-dependent measurements.

The two possible types of easy axes, $\langle 1\bar{1}0\rangle$ and $\langle 112\rangle$, should exhibit different temperature dependence of the intensity distribution when imaged, for instance, at $\alpha=0°$ [Fig. 2(a)]. For the case of a $\langle 1\bar{1}0\rangle$ preferred axis, the magnetic axis for the domains with the largest contrast [2 and 4 at dashed line e in Fig. 3(a)] is perpendicular to the electric field vector of the incident x rays. Thus, the difference between these two domains is dependent only on the contribution from ferroelectric polarization (P), which does not change appreciably over this temperature range.[29] However, in the case of a $\langle 112\rangle$ preferred axis, the axis is not perpendicular to the electric field vector of the x rays, and therefore a definite temperature dependence arising from the magnetic contribution to the dichroism can be expected. Equation (2) can be adapted to variable temperature measurements by requiring both P and Q to vary as a function of temperature. Recognizing that the ferroelectric polarization in BFO does not change appreciably over the temperature range from room temperature to the Néel temperature (~370 °C),[29] we focus on the temperature dependence of Q, which should go to zero at the Néel temperature.[23] From this, one can then estimate a ~40% reduction in total intensity at the Néel temperature (370 °C) and, by interpolation, a ~20% reduction in contrast should be achieved from room temperature to 200 °C. A full temperature dependence study to temperature above T_N is not essential as strong temperature dependent changes in contrast are observed well before that temperature.

Figure 4 illustrates the contrast between these domains (2—light gray and 4—black) that has been repeatedly taken at room temperature [Fig. 4(a)] and at 200 °C [Fig. 4(b)]. These images exhibit four shades—white, light gray, medium gray, and black. Light gray and black correspond to the domains with the largest contrast (domains 2 and 4), whose temperature dependence determines which magnetic axis is present. The medium gray is achieved for both 1 and 3 domains. As illustrated by the several 2/4 locations plotted in Fig. 4(c), the contrast was found to decrease by ~17% upon heating, which is in reasonable agreement with the $\langle 112\rangle$ easy-axis scenario. Continued contrast reduction was observed at higher temperatures but sample damage at these temperatures began to threaten sample integrity and therefore we have not included data beyond 200 °C. We have completed measurements on both films capped with a 2-nm-thick layer of SRO and uncapped BFO films preheated for 1 hour at 200 °C in an attempt to minimize the impact of any surface chemistry effects; however, the same trend as expected for the $\langle 112\rangle$ case was observed in all cases.

It is important to understand the driving force for this change in the magnetic structure in BFO. Strain-driven changes in magnetic structure have been observed previously in other magnetic oxide systems which exhibit a strong coupling among spin, charge, orbital, and lattice degrees of freedom. For example, strain has a strong effect on colossal magnetoresistance manganites. Strain-induced changes to the double-exchange ferromagnetism in these materials have been interpreted by considering the variation in the electronic hopping amplitude due to the change in bond lengths and bond angles.[30] Strain has also been shown to affect the nature of antiferromagnetic superexchange coupling in oxides such as NiO. Like BFO, NiO has an easy (111) magnetic plane. In the presence of strain, however, uniaxial anisotropy allows the formation of an easy axes with that plane, parallel to either [110] (nearest neighbor) or [112] (next nearest neighbor).[25] In NiO it has been suggested that an orthorhombic contraction (i.e., that which would result from an in-plane compressive strain) along [100] favors a $\langle 110\rangle$ easy axis; whereas a monoclinic expansion (i.e., that which would

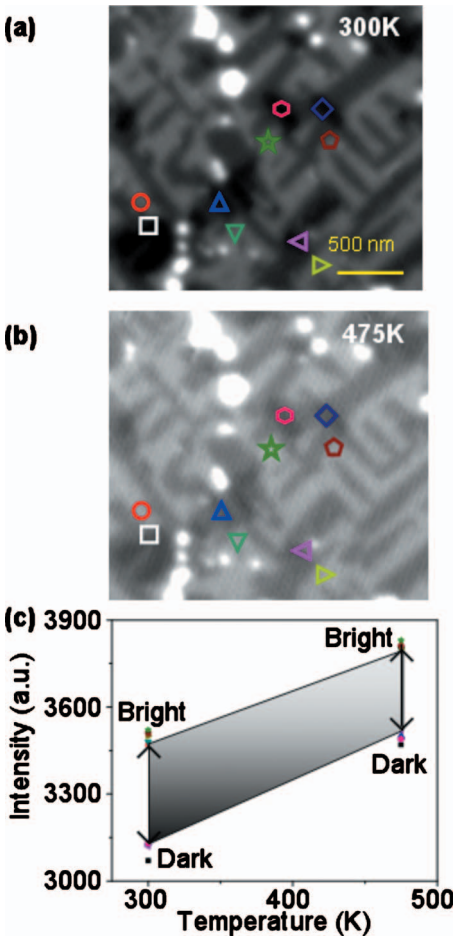

FIG. 4. (Color) Temperature-dependent dichroism measurements of BFO. XLD images taken at (a) room temperature and (b) 200 °C. The labeled spots in (a) and (b) represent a selection of locations used to probe the temperature-dependent change in dichoric contrast. (c) Temperature-dependent changes in intensity for type 2 and 4 domains for both temperatures reveals that the difference between the contrast from type 2 and 4 domains reduces by 17% at 200 °C. This is expected for the presence of a preferred magnetic [112] axis.

result from an in-plane tensile strain) along [110] favors a ⟨112⟩ easy axis.[31]

Epitaxial growth of BFO thin films on STO (001) substrates results in a similar strain effect on the antiferromagnetism. The lattice mismatch between BFO and STO (1.54%) imparts a compressive in-plane strain to the BFO film that is progressively relaxed as the film thickness is increased.[32] Using x-ray reciprocal-space mapping (RSM) of the 203 BFO diffraction peak as shown in Figs. 5(a) and 5(b) we have studied the strain state in such films as a function of film thickness. The in-plane (a) and out-of-plane (c) lattice parameters as well as the monoclinic tilt angle (β) are shown in the table along with a schematic describing the nature of the structural distortions [Figs. 5(c) and 5(d)]. In the case of a 200-nm-thick BFO/SRO/STO (001) film, the in-plane lattice parameters are matched with those of the substrate and the unit cell is under compressive strain ($c/a=1.039$) [Fig. 5(a)]. As the film thickness is increased to 1 μm, the lattice parameters gradually approach the bulk BFO value and the

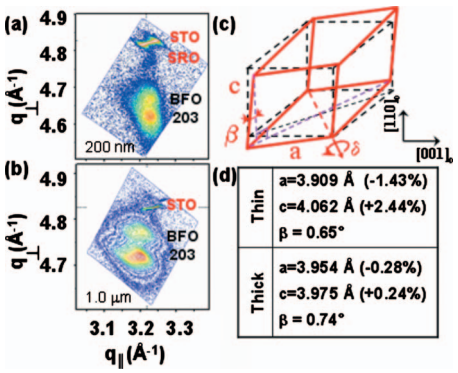

FIG. 5. (Color) The crystal structure of thin and thick BFO films grown on SRO/STO(001). RSMs for (a) thin and (b) thick BFO grown on SRO/STO(001). (c) Schematic illustrating the nature of the crystal structure of the BFO film, where a is the in-plane lattice parameter, c is the out-of-plane lattice parameter, and β is the monoclinic distortion angle. (d) Unit-cell parameters, as determined by RSM, for both strained (thin) and relaxed (thick) films.

pseudotetragonality ($c/a=1.005$) becomes smaller [Fig. 5(b)]. β is derived from the peak splitting of the 203 peak and is calculated to be ~0.74°, close to the value measured in bulk BFO. The in-plane compressive strain lifts the degeneracy of magnetization in the 111 plane, as is also observed in the case of NiO thin films.[25] This preferred axis can also be understood in terms of the magnetostriction in BFO. The magnetostriction constant of BFO is positive,[33] meaning that the lattice constants expand along an applied magnetic field. Substrate-induced compressive strain is effectively the opposite of this effect and thus results in a preference of a magnetization direction that has the largest out-of-plane component while remaining in the $(11\bar{1})$, i.e., the ⟨112⟩. This is consistent with the calculations for NiO, which has the opposite sign of magnetostriction from BFO, and therefore demonstrates the opposite preferential magnetic ⟨110⟩ axis when under compressive strain.[31] Additionally, preliminary findings suggest that BFO films under tensile strain (for example, by epitaxial growth on Si) have a $\langle 1\bar{1}0\rangle$ easy magnetic axis. This demonstrates that one can control the nature the magnetic axis in such multiferroic thin films and in turn use this ability to better engineer a new generation of devices that utilize electric field driven changes in magnetic order.

In conclusion, the evolution of magnetism in multiferroic BFO is clearly a complex and intriguing subject. Through a careful experimental and theoretical study of PEEM images and the underlying structure of BFO, we have determined that epitaxially strained thin films do not show a degenerate magnetic plane as predicted for bulk, but instead exhibit the formation of a preferred magnetic axis depending on the nature of strain (⟨112⟩ or $\langle 1\bar{1}0\rangle$ for compressive and tensile strain, respectively). In compressively strained BFO (001) thin films, the antiferromagnetic direction lies along the ⟨112⟩ axes. This axis points as far out of the surface plane as possible while remaining perpendicular to the polarization direction. The following polarization directions {$[11\bar{1}]$, $[1\bar{1}\bar{1}]$, $[\bar{1}1\bar{1}]$, and $[\bar{1}\bar{1}\bar{1}]$} have the corresponding axes {[112], $[1\bar{1}2]$, $[\bar{1}12]$, and $[\bar{1}\bar{1}2]$, respectively}. Thick films no longer

retain this preferred direction, instead showing a variation in the magnetic direction, consistent with the perpendicular easy plane behavior observed in bulk. These observations will enable a deeper understanding of the magnetic exchange interactions at an interface between such epitaxial BFO films and a ferromagnet and aid in the design of next generation devices.[34] Finally, we believe this x-ray dichroism based spectromicroscopy technique can be generically applied to other multiferroic systems where magnetic behavior has been difficult to determine due to the complexity of multiple order parameters and thus represents a powerful tool in achieving unprecedented understanding of order in these exciting materials.

This work has been supported by the Director, Office of Basic Energy Sciences, Materials Science Division of the U.S. Department of Energy under Contract No. DE-AC02-05CH11231. C.H.Y. was supported by a Korea Research Foundation Grant (MOEHRD) (KRF-2006-214-C00020). Y.H.C. would like to acknowledge the support of the National Science Council, R.O.C., under Contract No. NSC 98-2119-M-009-016.

*mikel.holcomb@mail.wvu.edu

[1] M. Fiebig, J. Phys. D **38**, R123 (2005).
[2] W. Eerenstein, N. D. Mathur, and J. F. Scott, Nature (London) **442**, 759 (2006).
[3] S.-W. Cheong and M. Mostovoy, Nature Mater. **6**, 13 (2007).
[4] R. Ramesh and N. A. Spaldin, Nature Mater. **6**, 21 (2007).
[5] H. Bea, M. Gajek, M. Bibes, and A. Barthelemy, J. Phys.: Condens. Matter **20**, 434221 (2008).
[6] P. Borisov, A. Hochstrat, X. Chen, W. Kleemann, and C. Binek, Phys. Rev. Lett. **94**, 117203 (2005).
[7] X. Martí, F. Sánchez, J. Fontcuberta, M. V. García-Cuenca, C. Ferrater, and M. Varela, J. Appl. Phys. **99**, 08P302 (2006).
[8] J. Dho, X. Qi, H. Kim, J. L. MacManus-Driscoll, and M. G. Blamire, Adv. Mater. **18**, 1445 (2006).
[9] V. Laukhin, V. Skumryev, X. Martí, D. Hrabovsky, F. Sánchez, M. V. García-Cuenca, C. Ferrater, M. Varela, U. Lüders, J. F. Bobo, and J. Fontcuberta, Phys. Rev. Lett. **97**, 227201 (2006).
[10] H. Béa, M. Bibes, F. Ott, B. Dupé, X. H. Zhu, S. Petit, S. Fusil, C. Deranlot, K. Bouzehouane, and A. Barthélémy, Phys. Rev. Lett. **100**, 017204 (2008).
[11] A. Pimenov, A. A. Mukhin, V. Yu. Ivanov, V. D. Travkin, A. M. Balbashov, and A. Loidl, Nat. Phys. **2**, 97 (2006).
[12] D. Lebeugle, D. Colson, A. Forget, M. Viret, A. M. Bataille, and A. Goukasov, Phys. Rev. Lett. **100**, 227602 (2008).
[13] C. A. F. Vaz, J. A. C. Bland, and G. Lauhoff, Rep. Prog. Phys. **71**, 056501 (2008).
[14] C. Michel, J.-M. Moreau, G. D. Acheubach, and W. J. James, Solid State Commun. **7**, 701 (1969).
[15] P. Fischer, M. Polomska, I. Sosnowska, and M. Szymanski, J. Phys. C **13**, 1931 (1980).
[16] S. V. Kiselev, R. P. Ozerov, and G. S. Zhdanov, Sov. Phys. Dokl. **7**, 742 (1963).
[17] S. Lisenkov, D. Rahmedov, and L. Bellaiche, Phys. Rev. Lett. **103**, 047204 (2009).
[18] I. E. Dzyaloshinskii, Sov. Phys. JETP **5**, 1259 (1957).
[19] T. Moriya, Phys. Rev. **120**, 91 (1960).
[20] C. Ederer and N. A. Spaldin, Phys. Rev. B **71**, 060401(R) (2005).
[21] F. Zavaliche, S. Y. Yang, T. Zhao, Y. H. Chu, M. P. Cruz, C. B. Eom, and R. Ramesh, Phase Transitions **79**, 991 (2006).
[22] J. Stohr and H. C. Siegmann, *Magnetism From Fundamentals to Nanoscale Dynamics* (Springer, New York, 2006).
[23] A. Scholl, H. Ohldag, F. Nolting, J. Stohr, and H. A. Padmore, Rev. Sci. Instrum. **73**, 1362 (2002).
[24] G. Cressy, C. M. B. Henderson, and G. van der Laan, Phys. Chem. Miner. **20**, 111 (1993).
[25] H. Ohldag, A. Scholl, F. Nolting, S. Anders, F. U. Hillebrecht, and J. Stohr, Phys. Rev. Lett. **86**, 2878 (2001).
[26] J. Stöhr, A. Scholl, T. J. Regan, S. Anders, J. Lüning, M. R. Scheinfein, H. A. Padmore, and R. L. White, Phys. Rev. Lett. **83**, 1862 (1999).
[27] T. Tsuboi, Phys. Rev. B **39**, 2842 (1989).
[28] G. van der Laan, E. Arenholz, R. V. Chopdekar, and Y. Suzuki, Phys. Rev. B **77**, 064407 (2008).
[29] T. Zhao, A. Scholl, F. Zavaliche, K. Lee, M. Barry, A. Doran, M. P. Cruz, Y. H. Chu, C. Ederer, N. A. Spaldin, R. R. Das, D. M. Kim, S. H. Baek, C. B. Eom, and R. Ramesh, Nature Mater. **5**, 823 (2006).
[30] A. J. Millis, A. Migliori, and T. Darling, J. Appl. Phys. **83**, 1588 (1998).
[31] T. Yamada, J. Phys. Soc. Jpn. **21**, 664 (1966).
[32] Y. H. Chu, T. Zhao, M. P. Cruz, Q. Zhan, P. L. Yang, L. W. Martin, M. Huijben, C. H. Yang, F. Zavaliche, H. Zheng, and R. Ramesh, Appl. Phys. Lett. **90**, 252906 (2007).
[33] A. K. Zvezdin, A. M. Kadomtseva, S. S. Krotov, A. P. Pyatakov, Yu. F. Popov, and G. P. Vorob'ev, J. Magn. Magn. Mater. **300**, 224 (2006).
[34] Y. H. Chu, L. W. Martin, M. B. Holcomb, M. Gajek, S.-J. Han, Q. He, N. Balke, C.-H. Yang, D. Lee, W. Hu, Q. Zhan, P.-L. Yang, A. Fraile-Rodriquez, A. Scholl, S. X. Wang, and R. Ramesh, Nature Mater. **7**, 478 (2008).